ACS APPLIED MATERIALS & INTERFACES

Research Article

Cite This: ACS Appl. Mater. Interfaces 2019, 11, 15498−15506

www.acsami.org

Micro-/Macroscopically Synergetic Control of Switchable 2D/3D Photothermal Water Purification Enabled by Robust, Portable, and Cost-Effective Cellulose Papers

Feng Ni,[†,‡] Peng Xiao,*[,†,‡] Chang Zhang,[†] Yun Liang,[†,‡] Jincui Gu,[†] Lei Zhang,*[,†,‡] and Tao Chen*[,†,‡]

[†]Key Laboratory of Marine Materials and Related Technologies, Zhejiang Key Laboratory of Marine Materials and Protective Technologies, Ningbo Institute of Materials Technology and Engineering, Chinese Academy of Sciences, Ningbo 315201, China

[‡]University of Chinese Academy of Sciences, 19A Yuquan Road, Beijing 100049, China

Supporting Information

ABSTRACT: Solar energy, as a renewable and sustainable resource, is considered to be a promising candidate for solving the water shortage through an interfacial solar-to-thermal conversion. Despite tremendous advances are achieved, it is still challenging for limited size, high-cost, and complicated fabrication protocols. More importantly, a favorable 2D/3D structure transformation to adapt to diverse conditions is considered to be very important. Inspired by the transformers with changeable geometries, herein, a large-area polypyrrole chemically functionalized cellulose paper (PPyP) with tunable microstructures and macroscopic geometries is developed via an in situ controlled oxypolymerization reaction. The resulted PPyP enables tunable 2D interfacial solar vaporization and even adapt itself to realization of 3D structures transformation for high-efficient water evaporation of up to 2.99 kg m^{-2} h^{-1} under 1 sun via an alternative kirigami/origami approach. Significantly, the PPyP can realize a switchable transformation between 2D and 3D structures to adapt diverse environments, demonstrating significant potentials in environmentally adaptable water purification.

KEYWORDS: *micro/macroscopically control, switchable 2D/3D water purification, interfacial photothermal conversion, low-cost, cellulose papers*

1. INTRODUCTION

With the rapid development of society and undesirable pollution, the shortage of fresh water has become a global concern that urgently needs to be settled.[1,2] Owing to the renewable and sustainable features, solar energy is considered to be a promising candidate for water purification.[3−5] Specifically, interfacial solar-to-thermal conversion with preferable efficiency has blossomed over the past few years.[6−11] Up to date, tremendous advances have been achieved, which enable a variety of photothermal materials to function as effective two-dimensional (2D) solar vapor generators, including nanoparticles enabled bilayer membranes,[12−15] carbon nanotubes (CNTs)/graphene-based films,[16−22] carbon-based aerogels,[23−28] bilayer woods,[29−34] hydrogels,[35−37] etc. More recently, owing to the efficient utilization of three-dimensional (3D) space and absorption of environmental enthalpy, 3D evaporators are considered to significantly enhance photothermal water purification capacity.[38−43] However, it is still challenging to achieve highly switchable 2D/3D structure to adapt diverse environmental conditions in a simple, low-cost, and effective way.

Cellulose paper that is ubiquitous in our daily life is an environmental-friendly, scalable, low-cost fibrous substrate, demonstrating excellently flexible, portable, and foldable properties.[44,45] On the basis of the desirable advantages, paper-based flexible electronics,[46] actuators,[47] and energy storage devices[48] are highly developed in recent years. Specifically, to combine with functional photothermal components, it can be further exploited to realize a robust, portable, and cost-effective photothermal water purification. Among various photothermal materials were investigated,[7,8] given the stability, costs, scalable production, and fabrication protocols, PPy is expected to be a good choice to function as light absorbers on cellulose papers for efficient water evaporation. In our system, PPy was expected to demonstrate favorable light absorption, strong interaction with cellulose fibers and facile preparation approaches.[37,42,49] Herein, we describe an editable, scalable, and efficient approach to fabricate polypyrrole modified paper (PPyP) via in situ oxypolymerization. Microscopically, the as-prepared PPyP demonstrated tunable microstructures, enabling well-controllable performance of water purification through balancing the

Received: January 7, 2019
Accepted: April 9, 2019
Published: April 9, 2019

DOI: 10.1021/acsami.9b00380
ACS Appl. Mater. Interfaces 2019, 11, 15498−15506

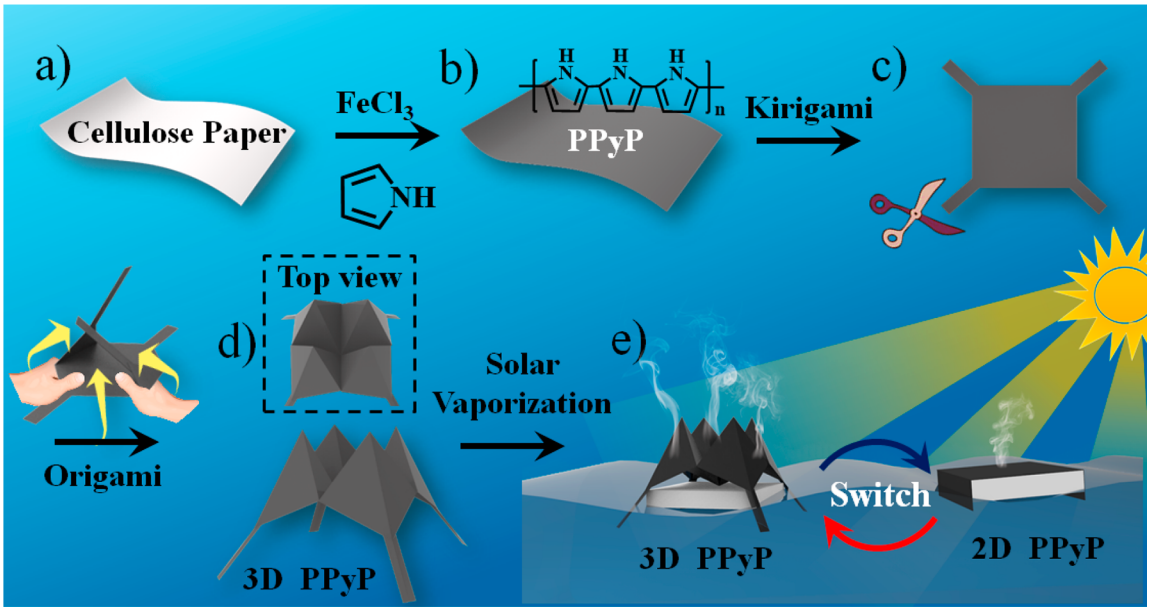

Figure 1. Schematic illustration of the preparing procedure of chemically functionalized cellulose papers with switchable 2D/3D structures. (a, b) The fabrication strategy of the PPyP. (c) Desired 2D shape by kirigami technique. (d) A 3D pyramid-like structure prepared via a kid's origami game called as cootie catcher. (e) Water-assisted switch of 2D and 3D PPyP.

two factors of light absorption and water transportation. Macroscopically, it can be further cut into desired shapes and subsequently folded into specific 3D architectures, which allows the high-efficient utilization of 3D space for enhanced photothermal water purification performance of 2.99 kg m^{-2} h^{-1} under 1 sun. Superior to the conventional fixed 3D structures, the paper-based one can experience cycled switch of 2D/3D state with preferable remolding capability, ensuring good university, and adaptability under diverse conditions.

2. EXPERIMENTAL SECTION

2.1. Materials and Chemicals. The cellulose paper we used was commercial printing paper that was from Fuji Xerox Co., Ltd. Ferric chloride ($FeCl_3 \cdot 6H_2O$), pyrrole monomer, and hydrochloric acid (HCl, 37%) were obtained from Sigma-Aldrich. All chemical products were of analytical grade and used without further treatment.

2.2. Preparation of PPyP. For the preparation of PPyP, a simple and scalable in situ oxypolymerization of pyrrole was adopted. Briefly, a piece of commercially available paper was first soaked in 1 M ferric chloride ($FeCl_3$) solution with 1 M hydrochloric acid (HCl) for 1 h, and then, it was transferred into the 0.2 M pyrrole monomer for different times of 15 min, 30 min, 45 min, 1 h, 2 h, 4 h, and 6 h. Here, we denoted these samples as P-0.25, P-0.5, P-0.75, P-1, P-2, P-4, and P-6, respectively. The as-fabricated papers were taken out and thoroughly rinsed with 1 M HCl and DI water, sequentially. The washed papers were kept in fume hood at room temperature (~25 °C) to dry it. Finally, the PPyP was obtained.

2.3. Preparation of Solar Absorber. 2D PPyP was prepared by attaching the as-prepared PPyP (2 cm × 5 cm) to a 10 mm-thick polystyrene (PS) foam (2 cm × 2 cm). Inspired by a kid's game named cootie catcher, 3D PPyP was prepared via a facile kirigami/origami-inspired method. At first, the as-prepared PPyP was cut into a specific shape, which was a square with four tails at its four corners. Second, four tails were folded to the center of square along the axis of symmetry. Third, the sample was flipped and its four corners were folded to its center. Then the sample's four corners were squeezed toward the center to get a 3D PPyP. Finally, the as-resulted 3D PPyP was fixed on top of PS foam with a thickness of 10 mm for solar-driven photothermal water purification.

2.4. Characterizations. The morphologies and microstructures of the as-prepared PPyP were observed by Field emission scanning electron microscope (FE-SEM) with a FE scanning electron microanalyzer (Hitachi-S4800, 4 kV). Fourier transform infrared spectra were obtained by an attenuated total reflection Fourier transformed Infrared Spectrometer (ATR-FTIR). The contact angle was carried out by a contact angle meter (DCAT21), using a 3 μL droplet as an indicator. The tensile strength was measured on universal material testing machine (Instron 5567). IR images and the corresponding temperatures were captured using the FLIR thermal camera. The concentrations of ions in the water samples were analyzed by inductively coupled plasma atomic emission spectroscopy (ICP-AES, NexION 300X). The reflection and transmittance were recorded using an ultraviolet−visible−near-infrared spectrophotometer equipped with an integrating sphere (Lambda 950). The absorption (A) was then calculated by $A = 1 - R - T$. Accordingly, the total solar absorptance (TSA) was calculated by the formula[10]

$$\mathrm{TSA} = \frac{\int_{\lambda_{\min}}^{\lambda_{\max}} (1 - R) S \, \mathrm{d}\lambda}{\int_{\lambda_{\min}}^{\lambda_{\max}} S \, \mathrm{d}\lambda} \quad (1)$$

where T and R are the transmission and reflection, respectively, S is the wavelength-dependent solar spectral irradiation (W m^{-2} nm^{-1}), and λ is the wavelength (nm).

2.5. Solar-Driven Photothermal Water Purification Experiment. The in-lab sunlight was provided Solar Simulator (HM-Xe500W) with standard AM 1.5 G solar irradiance density spectrum. The water evaporation rate was calculated based on the mass change (m) of water, which was accurately measured by using an electronic scale (GXG-JJ224BC). Then water evaporation rate (ER) and evaporation efficiency (η) were calculated by[36]

$$\mathrm{ER} = m/S_{\mathrm{p}} \quad (2)$$

$$\eta = \dot{m}(h_{\mathrm{v}} + C\dot{\Delta T})/S_{\mathrm{p}} q_{\mathrm{solar}} \quad (3)$$

where m (kg m^{-2} h^{-1}) is the mass change of water, S_{p} is the projected area of the solar absorber, $\dot{m}$ is the rate of water evaporation after subtracting evaporation rate under the dark environment, h_{v} is the enthalpy of vaporization (~2260 kJ kg^{-1}), C is the specific heat capacity of water and a constant of 4.18 J g^{-1} K^{-1}, ΔT is the

DOI: 10.1021/acsami.9b00380
ACS Appl. Mater. Interfaces 2019, 11, 15498−15506

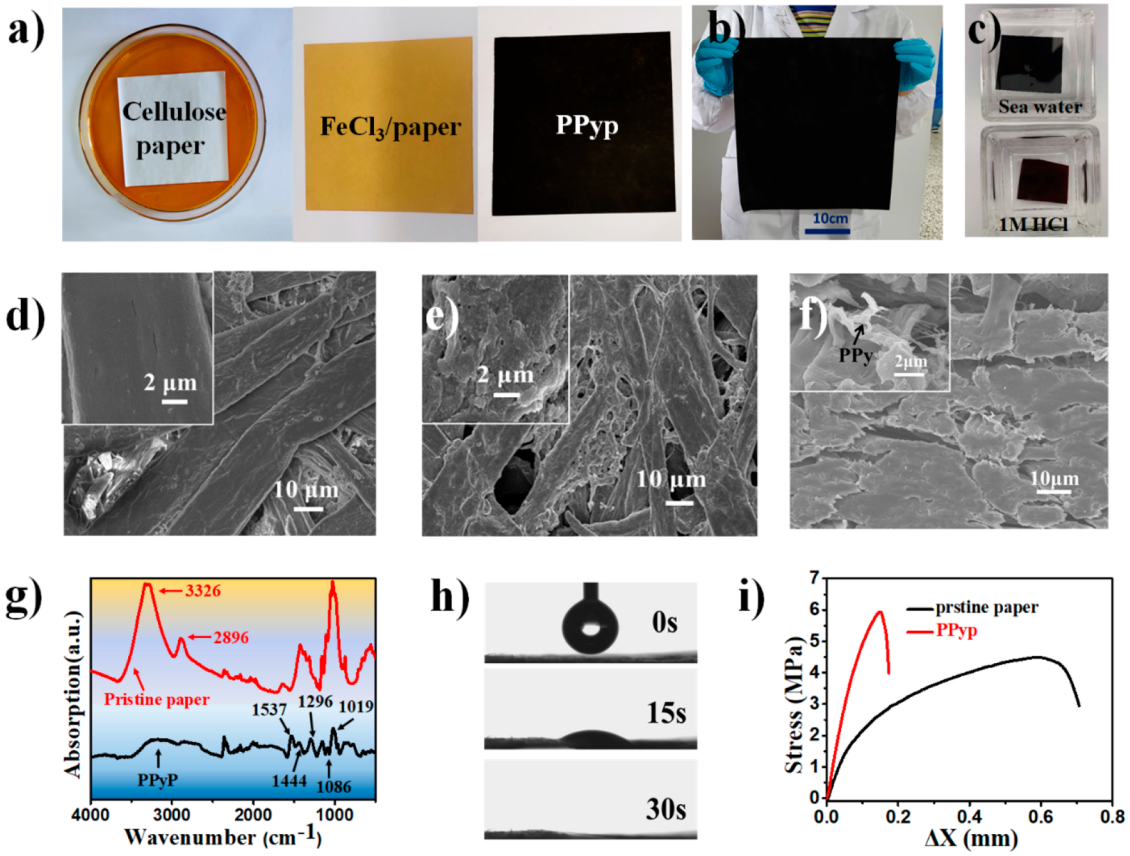

Figure 2. Fabrication and characterization of the as-fabricated PPyP. (a) The fabrication process of PPy/paper. (b) Physical picture of a large-scale piece (34 × 36 cm) of the as-prepared PPyP. (c) The PPyP was very stable in some extreme conditions. (d, e) SEM images of the pristine paper and the PPyP. The magnified views in the inset of panels d and e. (f) Cross-section-view image of the PPyP and the inset showing the existence of PPy. (g) Fourier transform infrared spectra of PPyP and pristine paper. (h) Contact angle of the PPyP. (i) Mechanical properties of the PPyP and pristine paper.

temperature increase of surface of the PPyP, and q_{solar} is the intensity of simulated solar light on the surface of the absorber. All in-lab measurements were conducted at an ambient temperature of 30 °C with humidity of 50%. In this manuscript, the outdoor experiments were carried out on the roof of the materials building of Ningbo Institute of Industrial Technology, CAS. The size of the outdoor prototype that was composed of poly(methyl methacrylate) (PMMA) was 13 cm × 13 cm × 30 cm. Additionally, projected areas of 2D and 3D PPyP absorber were both ~70 cm^2 in the outdoor experiment. The IR images were taken in the open system after the surface temperature reached to a stable state.

3. RESULTS AND DISCUSSION

As schematically illustrated in Figure 1, the commercially available cellulose paper with porous structures was adopted to act as a frame material, followed by subsequent ferric absorption and final PPy oxypolymerization (Figure 1a and 1b). The resulted PPyP represents flexible and preferable mechanical strength, which can be further tailored into desired shapes via kirigami and folded to 3D structure by origami technique (Figure 1c and 1d). As a proof of concept, owing to the desirable four pyramid-like geometries in one structure, a kid's origami game called as cootie catcher was selected in our system. Furthermore, the achieved 3D PPyP was then supported by a floated polystyrene (PS) foam with excellent thermal isolation property. Note that the as-prepared four tails by kirigami technique can further provide the smooth water channel for efficient interfacial solar vaporization. Importantly, the switchable 2D/3D PPyP could adapt to diverse environments by alternatively adjusting the geometries (Figure 1e).

The detailed fabrication procedure was displayed in Figure 2a. The facile and robust PPy deposition strategy allows the formation of a large-area PPyP with the lateral size of about 34 cm × 36 cm (Figure 2b). After appropriate annealing process, the PPy demonstrated excellent adhesion to the paper surface, resulting from high stability in some extreme conditions. As shown in Figure S1, the resulted paper composite can endure rigorous water rinsing procedure without any breakage. In addition, the stability tests were also conducted. When the PPyP was immersed into the seawater and 1 M HCl solution for at least 1 month, no obvious breakage was observed, which derived from the desirable antidissolution and antimelting features of the deposited PPy (Figure 2c). Microscopically, the microstructures of the paper before and after PPy modification were further characterized using SEM. As displayed in Figure 2d and 2e, compared with the smooth fibrous structure of the original paper, the PPy modified one demonstrated relatively rough surface with PPy polymer distributed on the fiber surface and embedded into the pores. The cross-sectional images in Figures 2f and S2 also evidenced the successful modification of the PPy. In addition, the chemical composition of the PPyP was further characterized using the ATR-FTIR. The bands located at ~1537, ~1086, and ~1019 cm^{-1} reflected C═C, C−C in-ring-stretching, and the C−H out-of-plane deformation vibration, respectively. The characteristic

DOI: 10.1021/acsami.9b00380
ACS Appl. Mater. Interfaces 2019, 11, 15498−15506

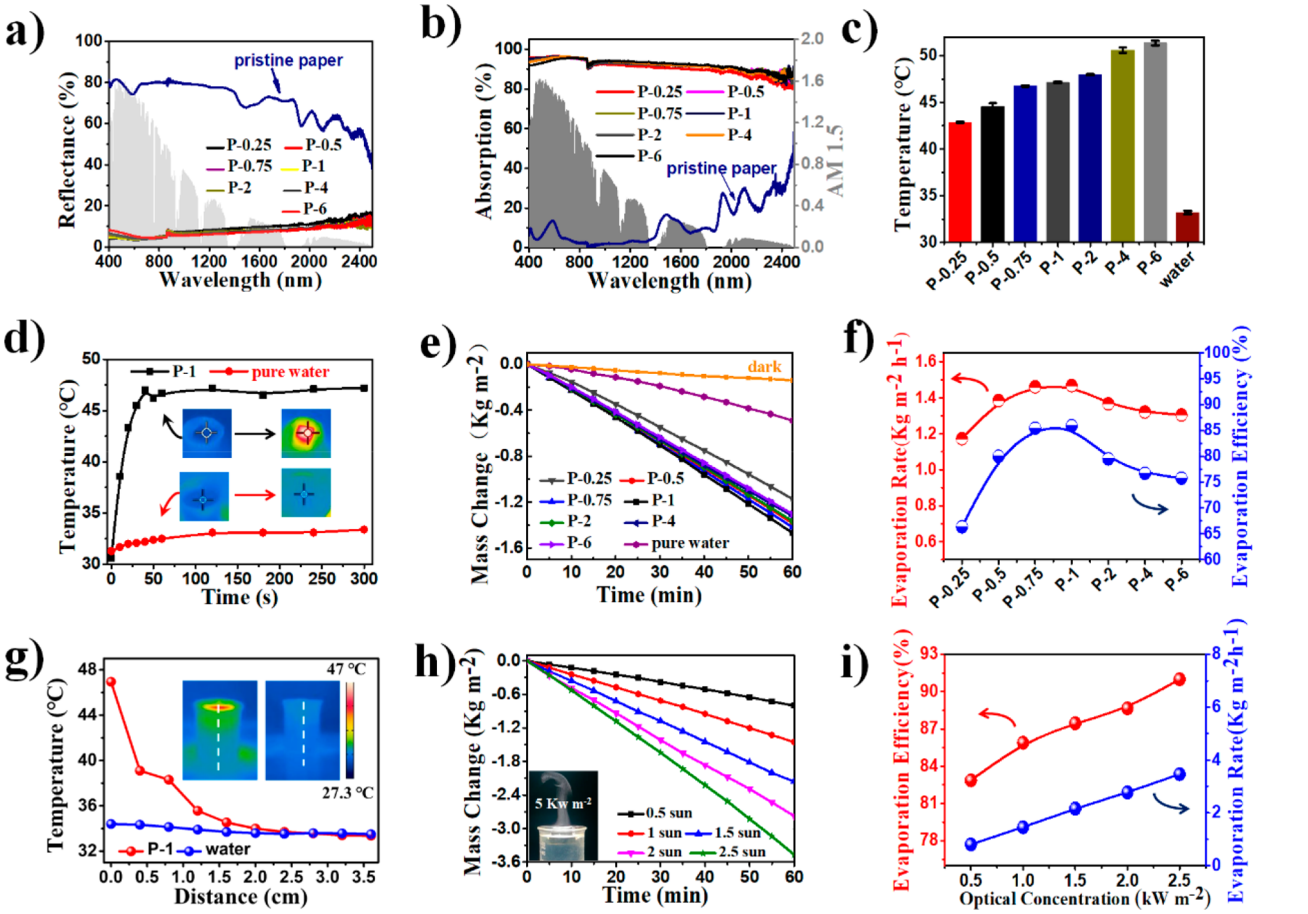

Figure 3. Optical, photothermal, and solar vapor generation performance of the as-fabricated PPyP. (a, b) Reflection and absorption spectra of different samples and pristine paper in the wavelength range of 400 to 2500 nm, and comparison with the standard AM 1.5G spectrum filter (gray, right-hand side axis). (c) T_e of different PPyP on the water/air interface and pure water under 1 sun. (d) Temperature change of P-1 and water as a function of irradiation time under 1 sun and the inset showing that IR thermal images of the initial and final states. (e) Mass change of the different PPyP and pure water under 1 kW m^{-2} illustration and dark condition over time. (f) Comparison of the evaporation rate and solar thermal evaporation efficiency among different samples under 1 sun. (g) Temperature profiles of the white marked lines in the inset image after 10 min light irradiation, and the inset pictures are IR thermal images of P-1 and pure water. (h) Mass change of P-1 under 1−2.5 kW m^{-2} illumination and the inset image demonstrating an enhanced steam generation by the P-1 under the solar illumination of 5 kW m^{-2}. (i) Evaporation rate and solar thermal conversion efficiency of P-1 under different solar irradiation varying from 1 to 2.5 sun.

peaks of C−N stretching vibration bands are at ∼1296 and ∼1444 cm^{-1}. These results strongly evidenced the successful functionalization of the PPy[50] (Figure 2g). It is noted that capability of water absorption of the solar absorbers can significantly affect the performance of the solar evaporation.[30] Water contact angle was further employed to explore the water absorption property. It can be found that the water droplet could be completely absorbed within 30 s, presenting excellent water transportation during the photothermal water purification process (Figure 2h). Besides, the PPy modified papers exhibited more hydrophilic than original paper, which was attributed to the nitrogen functional groups of PPy (Figure S3). More importantly, after modification, the mechanical strength of PPyP demonstrated remarkable improvement with a stress of 5.96 MPa (Figure 2i). The increase in stress after PPy coating is mainly derived from the high Young's modulus of PPy.

To explore the optimized performance of the PPyP, a series of experimental samples in different PPy deposition times of 0.25, 0.5, 0.75, 1, 2, 4, and 6 h were conducted in our system. From the UV−vis−IR absorption spectrum in Figure 3a, it can be observed that the reflectance of experimental samples is much lower than that of controlled sample (pristine paper). As a result, the solar absorption of these experimental samples demonstrated higher values than the controlled one (Figures 3b and S4). Note that the experimental samples demonstrated similar values of light absorption, where P-1 has 94.56% absorption of solar energy (weighted under AM1.5 G) in the wavelengths from 400 to 2500 nm ascribed to the characteristic broad-band absorption of PPy and enhanced light scattering of the rough surface of the PPyP. In order to further characterize the solar-to-thermal properties, the 2D solar steam generator system was selected in which the PPyP was adhered onto a floated PS foam surface at air/water interface with two tails immersed into the water subphase for continuous water pumping (Figure S5). As shown in Figure 3c, the equilibrium temperature (T_e) of these samples was conducted. With the increase of reaction time, the achieved temperature of the solar absorbers demonstrated an increase trend from ∼42.9 to ∼52.4 °C, which was much higher than that of the pure water with about ∼33 °C under 1 sun (Figures S6 and S7). Especially, the PPyP also demonstrated efficient photothermal conversion. Under 1 kW m^{-2} solar illumination, the temperature of P-1 quickly rose to 46.7 °C in 1 min

DOI: 10.1021/acsami.9b00380
ACS Appl. Mater. Interfaces 2019, 11, 15498−15506

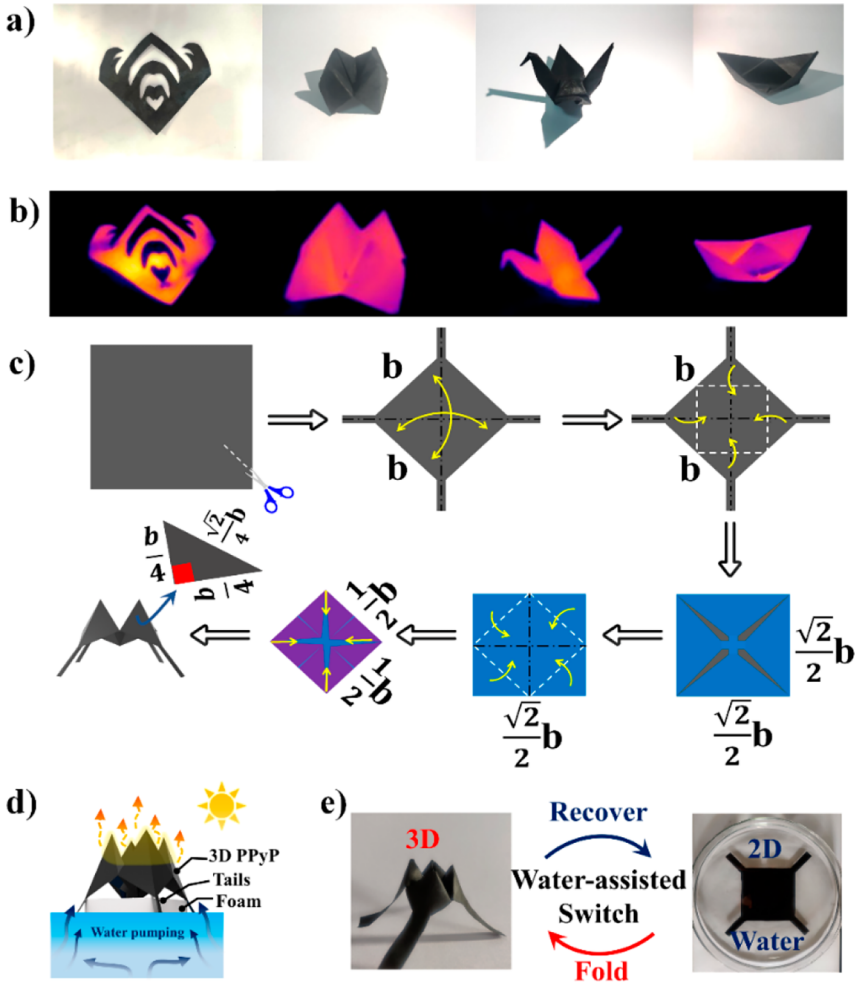

Figure 4. (a) Optical images and (b) IR thermal images under the 0.3 sun irradiation of different shapes via kirigami and origami of the PPyP. (c) Procedures of the 3D PPyP inspired by a kid's game named "cootie catcher" (the yellow arrows represented the direction of the folding, and the white dotted lines is the axis of symmetry of the folding). (d) Light-to-heat and water transport of the 3D PPyP. (e) Water-assisted switch of the 2D/3D PPyP.

(Figures 3d and S8). Since light absorption and water transportation are both essential factors that affect the solar vaporization, water evaporation experiments are further employed to investigate the optimized condition of the PPy deposition. As displayed in Figure 3e, the mass change of water is proportional to irradiation time under 1 sun equipped with AM 1.5G. Compared with pure water with an average value of 0.49 kg m^{-2} h^{-1}, the evaporation rate of PPyP in different reaction time initially increased and then decreased, which demonstrated a parabola-like trend. With the increase of reaction time, PPy was gradually deposited on the fiber surface, resulting in the corresponding reduction of capillary pores of the paper. Since the pores were blocked at certain reaction time, the water transportation was hindered, which could severely decrease the water evaporation (Figure S9). As a result, the P-1 exhibited the maximum evaporate rate of 1.47 kg m^{-2} h^{-1}. The evaporation efficiency of different PPyP under 1 sun illumination were measured in the Figure 3f, in which the solar-to-thermal efficiency of P-0.25, P-0.5, P-0.75, P-1, P-2, P-4, and P-6 were calculated to be 66.35%, 79.99%, 85.42%, 85.89%, 79.5%, 76.71%, and 75.76%, respectively. Additionally, the vertical temperature distribution was also investigated. Compared with the bulk water, the P-1 in Figure 3g strongly illustrated that the heat was strictly confined on the surface of the PPyP layer.

To further explore the adaptability and sustainability of the PPyP, simulated solar intensity ranging from 0.5 to 2.5 sun was employed to measure the performance of the photothermal water purification. The results showed that a continuous and stable water evaporation could be readily achieved and the evaporate rate of P-1 can reach up to 3.47 kg m^{-2} h^{-1} under 2.5 sun (Figure 3h). Similarly, the evaporation efficiency of P-1 also presented a consistent increase with the increase of solar intensity, in which a maximum evaporation efficiency of 91% under 2.5 sun is realized (Figure 3i). Furthermore, the PPyP has an excellent stability under intense ultraviolet light irradiation, which demonstrates significant potentials in water purification under long-term solar irradiation. (Figure S10).

Because of excellent tailorability and foldability, the as-prepared PPyP can be easily cut and folded into desired 2D and 3D architectures (Figure 4a). Upon solar light was applied on the fabricated structure, it can form distinct temperature gradient. IR images in Figure 4b provided remarkably colorful patterns, which coincided well with the optical images. Since the conventional 2D plane structure cannot effectively utilize the tridimensional space, a well-designed 3D structure is highly desired to realize an enhanced evaporation. As a proof of

DOI: 10.1021/acsami.9b00380
ACS Appl. Mater. Interfaces 2019, 11, 15498−15506

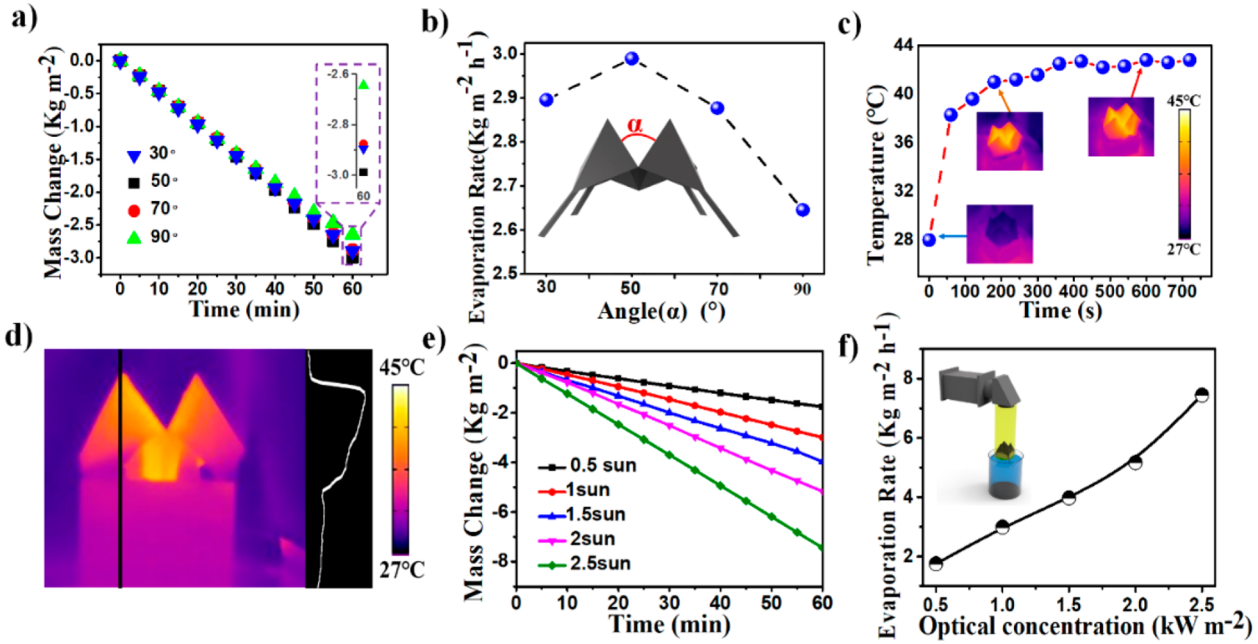

Figure 5. Photothermal and evaporation properties of 3D PPyP. (a) Mass changes of water of 3D PPyP with different α increasing from 30° to 90° under 1 sun. (b) Evaporation rate as a function of the angle between two adjacent pyramids under 1 sun. The inset show that schematic illustration of the angle between two adjacent pyramids. (c) Temperature of P-50 floating as a function of time under 1 sun. The insets of panel c are the IR thermal images of the P-50. (d) IR thermal image of 3D PPyP after solar irradiation for 600 s. Temperature profiles of the black marked line is in the right of the IR thermal image. (e, f) Mass change of water and evaporation rate with P-50 over time at different solar power densities increasing from 0.5 to 2.5 sun.

concept, a cootie catcher inspired 3D structure was fabricated in our system. First, a kirigami was used to tailor the PPyP into 2D structure with four tails for water pumping. The 2D paper was subsequently folded to 3D architecture with four pyramid-like architecture via origami strategy (Figures 4c and S11). Moreover, the 3D structure was integrated into a floated system with a polystyrene foam to minimize heat diffusion (Figure 4d).

The variable environmental condition allows the PPyP to experience the corresponding transformation between 2D and 3D structure to achieve desirable water evaporation. Specifically, two cases are considered in our system. Note that for the same piece of PPyP in 2D or 3D state, the amount of purified water is considered to be the key point in practical applications. When the area of the water surface available in the chamber is too small to accommodate most area of the unfolding 2D structure, the folded 3D one is preferred to realize a high-efficient water evaporation. Compared with the plain structure of 2D evaporator, the 3D one that efficiently utilized the vertical space represented remarkable increase of the effective water evaporation area for enhanced water purification (Figure S12a). However, when the water surface in a sealed chamber is big enough to accommodate the whole area of the unfolding 2D plane structure, the 2D one with more effective solar-radiation area than the 3D one is preferred and expected to absorb more solar energy for water purification (Figure S12b). Therefore, the 2D and 3D structures are deemed to both play important roles in the water evaporation toward the variable environment.

Nevertheless, after the origami/unfolding procedures, the PPyP could experience a transition from flat state to wrinkled one. Note that the wrinkled paper was not suitable for further 2D water evaporation. Water was regarded as an effective media to transform the wrinkled paper to a flat one. Because water molecules could effectively penetrate into the paper fibers and break interfibrous hydrogen bonds to make most of curved ones straighten again in a high temperature. Therefore, the process was named as a water assisted switch (WAS) (Figure 4e). Although the PPyP was rigorously folded several times, there were no obvious creases observed. Furthermore, the mechanical strength was still strong enough to support the 2D and 3D water evaporation experiments (Figures S13 and S14).

The evaporation rate of the 3D structure is calculated based on its projected area.[38,40,42,51] Additionally, the effective evaporation area of 3D structure is much larger than its projected area, which is similar to natural plants that extend themselves to the vertical space with hierarchical leaves for enhanced photosynthesis. As displayed in the Figure S15, it is the same for the effective evaporation area ($s_{e\alpha}$) and projected area ($s_{p\alpha}$) of 2D structure. However, the $s_{e\alpha}$ and $s_{p\alpha}$ of 3D PPyP depend on its length of square before folding (b) and the angle between two adjacent pyramids (α). Additionally, some areas of PPyP are overlapped during origami. As a result, $s_{e\alpha}$ and $s_{p\alpha}$ of 3D structure are described as $s_{e\alpha} = \frac{3}{4}b^2$, and $s_{p\alpha} = \frac{1}{8}\cos^2\left(\frac{\pi}{4} - \frac{\alpha}{4}\right)\cdot b^2 + \frac{\sqrt{3}}{8}b^2\cdot\cos\left(\frac{\pi}{4} - \frac{\alpha}{4}\right)$. Therefore, the angle between two adjacent pyramids can be readily adjusted to achieve well-controlled solar vaporization (Figure 5a). The ratio of $s_{e\alpha}$ to $s_{p\alpha}$ is defined as R. As presented by Figure S16, when α is 50°, R is 2.76. Furthermore, the concentrating effect between four pyramids and the reduction of thermal radiation can synergistically enhance the evaporation rate for 3D PPyP. As a result, the evaporation of P-50 can reach up to a maximum of 2.99 kg m^{-2} h^{-1} under 1 sun (Figures 5b and S19). As revealed in Table S1, this result was superior to most of pervious reports. The IR images of P-50 were also taken, in

DOI: 10.1021/acsami.9b00380
ACS Appl. Mater. Interfaces 2019, 11, 15498−15506

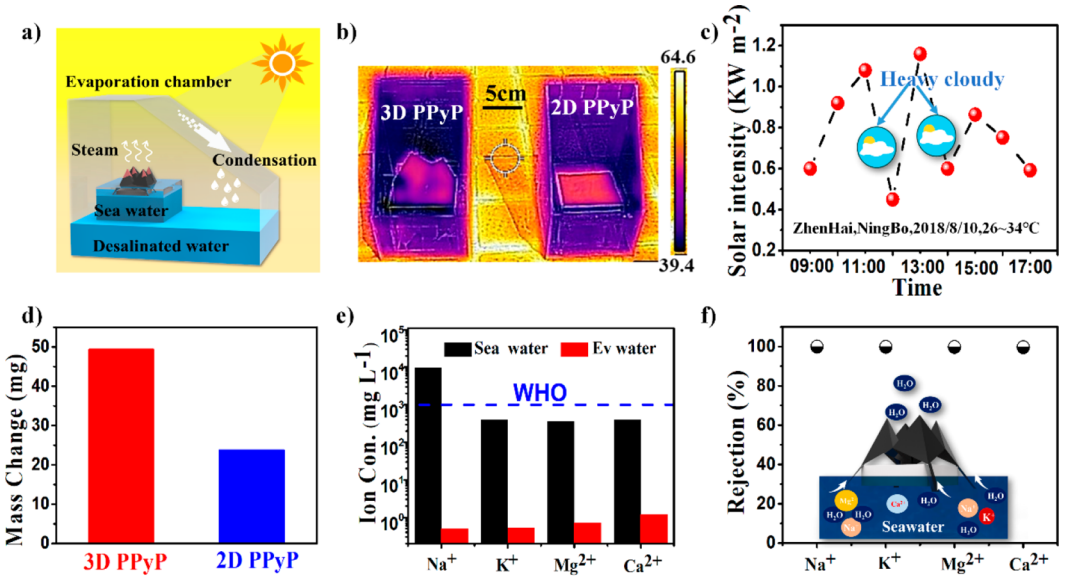

Figure 6. (a) Schematic configuration of outdoor evaporation for water purification. (b) IR thermal images of parallel experiment of 3D and 2D PPyP under natural solar light irradiation. (c) Solar intensity recorded over time on a heavy cloudy day from 9:00 to 5:00 pm (2018.8.10). (d) Mass change of pure water of 3D and 2D PPyP after 1 day of outdoor evaporation. (e) Measured concentration of four primary ions before and after desalination with 3D PPyP. The dashed lines represent the WHO standard for drinking water. (f) Rejection of four primary ions after desalination with 3D PPyP. The inset is the schematic illustration of desalination.

which the surface temperature rose to an equilibrium temperature of approximate 42.8 °C within 600 s under 1 sun (Figures 5c and S18). In addition, the vertical temperature distribution was measured using IR image, resulting in solar-to-thermal conversion confined in the 3D structure other than the water subphase (Figure 5d). When illuminated under different solar intensity of 0.5, 1, 1.5, 2, and 2.5 sun, it was found that the 3D generator can have a positively increase of evaporation rate with 1.75, 2.99, 3.97, 5.17, and 7.44 kg m^{-2} h^{-1} (Figure 5e and 5f). The result manifested that even the folded 3D system can under some extreme conditions, demonstrating significant potentials in developing portable and tunable photothermal water purification device. Since the 3D structure provides a robust platform for enhanced 3D evaporation, the capability of continuous work under diverse conditions is also considered. As displayed in Figure S20a, even if it supported an object with the weight ~7 times heavier than its own weight, the water-wicking PPyP did not undergo a distinct deformation. Furthermore, when the 3D PPyP device was put into the chamber with unevaporated water for 10 days, it still maintained the initial structure without any structural damage, demonstrating significant potentials in long-term operation (Figure S20b).

To investigate the potentials of practical application, outdoor experiments were conducted using a homemade device, which is schematically displayed in Figure 6a. In our system, controlled 2D and experimental 3D structures with same projected area are adopted to have a parallel experiment (Figure S21). IR image showed that the 3D structure demonstrated lower temperature than that of the 2D one, which derived from more thermal loss of 2D structure toward the ambient environment (Figure 6b).[52,53] The outdoor solar intensity ranging from 450 to 1160 W m^{-2}, and the average solar intensity is ~0.78 kW m^{-2} (Figure 6c). It is could be clearly seen that steam was quickly appeared in the sealed chamber in 10 s and condensed into water droplets and slides down in 5 min (Figure S22). As expected, the mass change of pure water with 3D structure was about 50 mL after 8 h under natural sunlight illumination (~6.9 L/m^{-2} day^{-1}), which was 2.2 times than that of 2D one (Figure 6d). To evaluate the performance of desalination, inductively coupled plasma atomic emission spectrometry (ICP-AES) was used to characterize the ions content of the purified water. It was found that the residual concentration of four primary ions (Na^+, K^+, Ca^{2+}, Mg^{2+}) were 3 orders of magnitude below the WHO standard for drinking water after sunlight irradiation (Figure 6e and Table S2). The calculated rejection of four primary ions after desalination is more than 99% (Figure 6f). Salt-containment is considered to be an important problem for continuous and high-efficient water evaporation.[54] Specifically, the 3D PPyP also demonstrates a favorable salt-rejecting capability (Figure S23). As a result, this well-designed 3D evaporation can significantly enhance the solar-to-thermal conversion, providing a new avenue for portable, foldable and efficient seawater distillation and sewage treatment.

4. CONCLUSIONS

In summary, we have developed a flexible and tailorable paper-based PPy hybrid with adjustable switch between 2D and 3D structures toward high-efficient water purification capacity. A in situ oxypolymerization approach enables the commercially available paper to realize uniform functionalization of PPy polymer. Microscopically, the water evaporation rate of 2D PPyP can be readily adjusted up to 1.47 kg m^{-2} h^{-1} under 1 sun by changing the reaction time. Macroscopically, inspired by a kid's game called as cootie catcher, an integrated kirigami/origami allows the transition from 2D to 3D solar evaporator to fully utilize the 3D space. The achieved 3D structure is highly tunable and shows an optimized water evaporation rate of up to 2.99 kg m^{-2} h^{-1} under 1 sun, demonstrating significant potentials in improving the solar-to-thermal conversion in a robust, low-cost and accessible way. Compared to conventional fixed 3D structure, this paper-based generator can easily and

DOI: 10.1021/acsami.9b00380
ACS Appl. Mater. Interfaces 2019, 11, 15498−15506

quickly switch between 2D/3D to better meet diverse evaporation needs.

■ ASSOCIATED CONTENT

Supporting Information

The Supporting Information is available free of charge on the ACS Publications website at DOI: 10.1021/acsami.9b00380.

Stability test of PPyP, cross-sectional SEM image of P-1, contact angle of the pristine paper, optical properties of dry-state PPyP and wet-state PPyP, schematic illustration of the 2D solar steam generation system, IR thermal images, the stability of PPyP under UV, photographs of the 3D PPyP at different views, schematic diagram of 2D/3D switch to adapt to different environment conditions, photos and mechanical property of PPyP after WAS, the relationship between the effective area and projected area of 2D and 3D structure, and parallel experiment of controlled 2D and experimental 3D structures and evaporation performance of the state-of-the-art devices in literatures and this work (PDF)

■ AUTHOR INFORMATION

Corresponding Authors

*E-mail: tao.chen@nimte.ac.cn.
*E-mail: xiaopeng@nimte.ac.cn.
*E-mail: zhanglei@nimte.ac.cn.

ORCID

Peng Xiao: 0000-0003-2231-9824
Tao Chen: 0000-0001-9704-9545

Author Contributions

The manuscript was written through contributions of all authors. All authors have given approval to the final version of the manuscript.

Notes

The authors declare no competing financial interest.

■ ACKNOWLEDGMENTS

We thank the Natural Science Foundation of China (51803226, 51573203), Key Research Program of Frontier Sciences, Chinese Academy of Sciences (QYZDB-SSW-SLH036), Postdoctoral Innovation Talent Support Program (BX20180321), China Postdoctoral Science Foundation (2018M630695), and Ningbo Science and Technology Bureau (2018A610108).

■ REFERENCES

(1) Elimelech, M.; Phillip, W. A. The Future of Seawater Desalination: Energy, Technology, and the Environment. *Science* **2011**, *333* (6043), 712−717.

(2) Kalogirou, S. A. Seawater Desalination Using Renewable Energy Sources. *Prog. Energy Combust. Sci.* **2005**, *31* (3), 242−281.

(3) Lewis, N. S. Research Opportunities to Advance Solar Energy Utilization. *Science* **2016**, *351* (6271), aad1920.

(4) Crabtree, G. W.; Lewis, N. S. Solar Energy Conversion. *Phys. Today* **2007**, *60* (3), 37−42.

(5) Cavusoglu, A.-H.; Chen, X.; Gentine, P.; Sahin, O. Potential for Natural Evaporation As A Reliable Renewable Energy Resource. *Nat. Commun.* **2017**, DOI: 10.1038/s41467-017-00581-w.

(6) Deng, Z.; Zhou, J.; Miao, L.; Liu, C.; Peng, Y.; Sun, L.; Tanemura, S. The Emergence of Solar Thermal Utilization: Solar-driven Steam Generation. *J. Mater. Chem. A* **2017**, *5* (17), 7691−7709.

(7) Tao, P.; Ni, G.; Song, C.; Shang, W.; Wu, J.; Zhu, J.; Chen, G.; Deng, T. Solar-Driven Interfacial Evaporation. *Nat. Energy* **2018**, *3*, 1031.

(8) Gao, M.; Zhu, L.; Peh, C. K.; Ho, G. W. Solar Absorber Material and System Designs for Photothermal Water Vaporization towards Clean Water and Energy Production. *Energy Environ. Sci.* **2019**, *12*, 841.

(9) Zhang, P.; Liao, Q.; Yao, H.; Huang, Y.; Cheng, H.; Qu, L. Direct Solar Steam Generation System for Clean Water Production. *Energy Storage Mater.* **2019**, *18*, 429.

(10) Zhu, L.; Gao, M.; Peh, C. K. N.; Ho, G. W. Solar-driven Photothermal Nanostructured Materials Designs and Prerequisites for Evaporation and Catalysis Applications. *Mater. Horiz.* **2018**, *5* (3), 323−343.

(11) Ghasemi, H.; Ni, G.; Marconnet, A. M.; Loomis, J.; Yerci, S.; Miljkovic, N.; Chen, G. Solar Steam Generation by Heat Localization. *Nat. Commun.* **2014**, *5*, 4449.

(12) Liu, Y.; Yu, S.; Feng, R.; Bernard, A.; Liu, Y.; Zhang, Y.; Duan, H.; Shang, W.; Tao, P.; Song, C.; Deng, T. A Bioinspired, Reusable, Paper-Based System for High-Performance Large-Scale Evaporation. *Adv. Mater.* **2015**, *27* (17), 2768−2774.

(13) Yang, Y.; Yang, X.; Fu, L.; Zou, M.; Cao, A.; Du, Y.; Yuan, Q.; Yan, C.-H. Two-Dimensional Flexible Bilayer Janus Membrane for Advanced Photothermal Water Desalination. *Acs Energy Lett.* **2018**, *3* (5), 1165−1171.

(14) Zhang, X.; Gao, W.; Su, X.; Wang, F.; Liu, B.; Wang, J.-J.; Liu, H.; Sang, Y. Conversion of Solar Power to Chemical Energy Based on Carbon Nanoparticle Modified Photo-thermoelectric Generator and Electrochemical Water Splitting System. *Nano Energy* **2018**, *48*, 481−488.

(15) Chang, C.; Yang, C.; Liu, Y.; Tao, P.; Song, C.; Shang, W.; Wu, J.; Deng, T. Efficient Solar-Thermal Energy Harvest Driven by Interfacial Plasmonic Heating-Assisted Evaporation. *ACS Appl. Mater. Interfaces* **2016**, *8* (35), 23412−23418.

(16) Wang, Y.; Wang, C.; Song, X.; Megarajan, S. K.; Jiang, H. A Facile Nanocomposite Strategy to Fabricate a RGO-MWCNT Photothermal Layer for Efficient Water Evaporation. *J. Mater. Chem. A* **2018**, *6* (3), 963−971.

(17) Yin, Z.; Wang, H.; Jian, M.; Li, Y.; Xia, K.; Zhang, M.; Wang, C.; Wang, Q.; Ma, M.; Zheng, Q.-s.; Zhang, Y. Extremely Black Vertically Aligned Carbon Nanotube Arrays for Solar Steam Generation. *ACS Appl. Mater. Interfaces* **2017**, *9* (34), 28596−28603.

(18) Yang, J.; Pang, Y.; Huang, W.; Shaw, S. K.; Schiffbauer, J.; Pillers, M. A.; Mu, X.; Luo, S.; Zhang, T.; Huang, Y.; Li, G.; Ptasinska, S.; Lieberman, M.; Luo, T. Functionalized Graphene Enables Highly Efficient Solar Thermal Steam Generation. *ACS Nano* **2017**, *11* (6), 5510−5518.

(19) Li, X.; Xu, W.; Tang, M.; Zhou, L.; Zhu, B.; Zhu, S.; Zhu, J. Graphene Oxide-based Efficient and Scalable Solar Desalination Under One Sun With a Confined 2D Water Path. *Proc. Natl. Acad. Sci. U. S. A.* **2016**, *113* (49), 13953−13958.

(20) Yang, Y.; Zhao, R.; Zhang, T.; Zhao, K.; Xiao, P.; Ma, Y.; Ajayan, P. M.; Shi, G.; Chen, Y. Graphene-Based Standalone Solar Energy Converter for Water Desalination and Purification. *ACS Nano* **2018**, *12* (1), 829−835.

(21) Zhang, P.; Li, J.; Lv, L.; Zhao, Y.; Qu, L. Vertically Aligned Graphene Sheets Membrane for Highly Efficient Solar Thermal Generation of Clean Water. *ACS Nano* **2017**, *11* (5), 5087−5093.

(22) Guo, A.; Ming, X.; Fu, Y.; Wang, G.; Wang, X. Fiber-Based, Double-Sided, Reduced Graphene Oxide Films for Efficient Solar Vapor Generation. *ACS Appl. Mater. Interfaces* **2017**, *9* (35), 29958−29964.

(23) Jiang, F.; Liu, H.; Li, Y.; Kuang, Y.; Xu, X.; Chen, C.; Huang, H.; Jia, C.; Zhao, X.; Hitz, E.; Zhou, Y.; Yang, R.; Cui, L.; Hu, L. Lightweight, Mesoporous, and Highly Absorptive All-Nanofiber Aerogel for Efficient Solar Steam Generation. *ACS Appl. Mater. Interfaces* **2018**, *10* (1), 1104−1112.

DOI: 10.1021/acsami.9b00380
ACS Appl. Mater. Interfaces 2019, 11, 15498−15506

(24) Mu, P.; Zhang, Z.; Bai, W.; He, J.; Sun, H.; Zhu, Z.; Liang, W.; Li, A. Superwetting Monolithic Hollow-Carbon-Nanotubes Aerogels with Hierarchically Nanoporous Structure for Efficient Solar Steam Generation. *Adv. Energy Mater.* **2019**, *9*, 1802158.
(25) Zhang, P.; Liao, Q.; Zhang, T.; Cheng, H.; Huang, Y.; Yang, C.; Li, C.; Jiang, L.; Qu, L. High Throughput of Clean Water Excluding Ions, Organic Media, and Bacteria From Defect-abundant Graphene Aerogel Under Sunlight. *Nano Energy* **2018**, *46*, 415−422.
(26) Fu, Y.; Wang, G.; Ming, X.; Liu, X.; Hou, B.; Mei, T.; Li, J.; Wang, J.; Wang, X. Oxygen Plasma Treated Graphene Aerogel As a Solar Absorber for Rapid And Efficient Solar Steam Generation. *Carbon* **2018**, *130*, 250−256.
(27) Jiang, Q.; Tian, L.; Liu, K.-K.; Tadepalli, S.; Raliya, R.; Biswas, P.; Naik, R. R.; Singamaneni, S. Bilayered Biofoam for Highly Efficient Solar Steam Generation. *Adv. Mater.* **2016**, *28* (42), 9400−9407.
(28) Wu, Y.; Yi, N.; Huang, L.; Zhang, T.; Fang, S.; Chang, H.; Li, N.; Oh, J.; Lee, J. A.; Kozlov, M.; Chipara, A. C.; Terrones, H.; Xiao, P.; Long, G.; Huang, Y.; Zhang, F.; Zhang, L.; Lepro, X.; Haines, C.; Lima, M. D.; Lopez, N. P.; Rajukumar, L. P.; Elias, A. L.; Feng, S.; Kim, S. J.; Narayanan, N. T.; Ajayan, P. M.; Terrones, M.; Aliev, A.; Chu, P.; Zhang, Z.; Baughman, R. H.; Chen, Y. Three-Dimensionally Bonded Spongy Graphene Material With Super Compressive Elasticity And Near-zero Poisson's Ratio. *Nat. Commun.* **2015**, DOI: 10.1038/ncomms7141.
(29) Jia, C.; Li, Y.; Yang, Z.; Chen, G.; Yao, Y.; Jiang, F.; Kuang, Y.; Pastel, G.; Xie, H.; Yang, B.; Das, S.; Hu, L. Rich Mesostructures Derived from Natural Woods for Solar Steam Generation. *Joule* **2017**, *1* (3), 588−599.
(30) Zhu, M.; Li, Y.; Chen, G.; Jiang, F.; Yang, Z.; Luo, X.; Wang, Y.; Lacey, S. D.; Dai, J.; Wang, C.; Jia, C.; Wan, J.; Yao, Y.; Gong, A.; Yang, B.; Yu, Z.; Das, S.; Hu, L. Tree-Inspired Design for High-Efficiency Water Extraction. *Adv. Mater.* **2017**, *29* (44), 1704107.
(31) Li, T.; Liu, H.; Zhao, X.; Chen, G.; Dai, J.; Pastel, G.; Jia, C.; Chen, C.; Hitz, E.; Siddhartha, D.; Yang, R.; Hu, L. Scalable and Highly Efficient Mesoporous Wood-Based Solar Steam Generation Device: Localized Heat, Rapid Water Transport. *Adv. Funct. Mater.* **2018**, *28* (16), 1707134.
(32) Chen, C.; Li, Y.; Song, J.; Yang, Z.; Kuang, Y.; Hitz, E.; Jia, C.; Gong, A.; Jiang, F.; Zhu, J. Y.; Yang, B.; Xie, J.; Hu, L. Highly Flexible and Efficient Solar Steam Generation Device. *Adv. Mater.* **2017**, *29* (30), 1701756.
(33) Zhu, M.; Li, Y.; Chen, F.; Zhu, X.; Dai, J.; Li, Y.; Yang, Z.; Yan, X.; Song, J.; Wang, Y.; Hitz, E.; Luo, W.; Lu, M.; Yang, B.; Hu, L. Plasmonic Wood for High-Efficiency Solar Steam Generation. *Adv. Energy Mater.* **2018**, *8* (4), 1701028.
(34) Kim, K.; Yu, S.; An, C.; Kim, S.-W.; Jang, J.-H. Mesoporous Three-Dimensional Graphene Networks for Highly Efficient Solar Desalination under 1 sun Illumination. *ACS Appl. Mater. Interfaces* **2018**, *10* (18), 15602−15608.
(35) Yin, X.; Zhang, Y.; Guo, Q.; Cai, X.; Xiao, J.; Ding, Z.; Yang, J. Macroporous Double-Network Hydrogel for High-Efficiency Solar Steam Generation Under 1 sun Illumination. *ACS Appl. Mater. Interfaces* **2018**, *10* (13), 10998−11007.
(36) Zhou, X.; Zhao, F.; Guo, Y.; Zhang, Y.; Yu, G. A Hydrogel-based Antifouling Solar Evaporator for Highly Efficient Water Desalination. *Energy Environ. Sci.* **2018**, *11*, 1985−1992.
(37) Zhao, F.; Zhou, X.; Shi, Y.; Qian, X.; Alexander, M.; Zhao, X.; Mendez, S.; Yang, R.; Qu, L.; Yu, G. Highly Efficient Solar Vapour Generation Via Hierarchically Nanostructured Gels. *Nat. Nanotechnol.* **2018**, *13* (6), 489−495.
(38) Hong, S.; Shi, Y.; Li, R.; Zhang, C.; Jin, Y.; Wang, P. Nature-Inspired, 3D Origami Solar Steam Generator toward Near Full Utilization of Solar Energy. *ACS Appl. Mater. Interfaces* **2018**, *10*, 28517−28524.
(39) Li, X.; Li, J.; Lu, J.; Xu, N.; Chen, C.; Min, X.; Zhu, B.; Li, H.; Zhou, L.; Zhu, S.; Zhang, T.; Zhu, J. Enhancement of Interfacial Solar Vapor Generation by Environmental Energy. *Joule* **2018**, *2* (7), 1331−1338.
(40) Li, X.; Lin, R.; Ni, G.; Xu, N.; Hu, X.; Zhu, B.; Lv, G.; Li, J.; Zhu, S.; Zhu, J. Three-dimensional Artificial Transpiration for Efficient Solar Waste-water Treatment. *Natl. Sci. Rev.* **2018**, *5* (1), 70−77.
(41) Shi, Y.; Li, R.; Jin, Y.; Zhuo, S.; Shi, L.; Chang, J.; Hong, S.; Ng, K.-C.; Wang, P. A 3D Photothermal Structure toward Improved Energy Efficiency in Solar Steam Generation. *Joule* **2018**, *2* (6), 1171−1186.
(42) Wang, Y.; Wang, C.; Song, X.; Huang, M.; Megarajan, S. K.; Shaukat, S. F.; Jiang, H. Improved Light-harvesting and Thermal Management for Efficient Solar-driven Water Evaporation Using 3D Photothermal Cones. *J. Mater. Chem. A* **2018**, *6* (21), 9874−9881.
(43) Zhang, P.; Liao, Q.; Yao, H.; Cheng, H.; Huang, Y.; Yang, C.; Jiang, L.; Qu, L. Three-dimensional Water Evaporation on a Macroporous Vertically Aligned Graphene Pillar Array Under One Sun. *J. Mater. Chem. A* **2018**, *6* (31), 15303−15309.
(44) Hu, L.; Choi, J. W.; Yang, Y.; Jeong, S.; La Mantia, F.; Cui, L. F.; Cui, Y. Highly Conductive Paper for Energy-storage Devices. *Proc. Natl. Acad. Sci. U. S. A.* **2009**, *106* (51), 21490−21494.
(45) Yao, B.; Zhang, J.; Kou, T.; Song, Y.; Liu, T.; Li, Y. Paper-Based Electrodes for Flexible Energy Storage Devices. *Adv. Sci.* **2017**, *4*, 1700107.
(46) Zhong, Q.; Zhong, J.; Cheng, X.; Yao, X.; Wang, B.; Li, W.; Wu, N.; Liu, K.; Hu, B.; Zhou, J. Paper-Based Active Tactile Sensor Array. *Adv. Mater.* **2015**, *27* (44), 7130−7136.
(47) Martinez, R. V.; Fish, C. R.; Chen, X.; Whitesides, G. M. Elastomeric Origami: Programmable Paper-Elastomer Composites as Pneumatic Actuators. *Adv. Funct. Mater.* **2012**, *22* (7), 1376−1384.
(48) Liu, A.; Kovacik, P.; Peard, N.; Tian, W.; Goktas, H.; Lau, J.; Dunn, B.; Gleason, K. K. Monolithic Flexible Supercapacitors Integrated into Single Sheets of Paper and Membrane via Vapor Printing. *Adv. Mater.* **2017**, *29* (19), 1606091.
(49) Zhang, L.; Tang, B.; Wu, J.; Li, R.; Wang, P. Hydrophobic Light-to-Heat Conversion Membranes with Self-Healing Ability for Interfacial Solar Heating. *Adv. Mater.* **2015**, *27* (33), 4889−4894.
(50) Yuan, L.; Yao, B.; Hu, B.; Huo, K.; Chen, W.; Zhou, J. Polypyrrole-Coated Paper for Flexible Solid-state Energy Storage. *Energy Environ. Sci.* **2013**, *6* (2), 470−476.
(51) Deng, Z.; Miao, L.; Liu, P.-F.; Zhou, J.; Wang, P.; Gu, Y.; Wang, X.; Cai, H.; Sun, L.; Tanemura, S. Extremely High Water-production Created by a Nanoink-stained PVA Evaporator With Embossment Structure. *Nano Energy* **2019**, *55*, 368−376.
(52) Song, H.; Liu, Y.; Liu, Z.; Singer, M. H.; Li, C.; Cheney, A. R.; Ji, D.; Zhou, L.; Zhang, N.; Zeng, X.; Bei, Z.; Yu, Z.; Jiang, S.; Gan, Q. Cold Vapor Generation beyond the Input Solar Energy Limit. *Adv. Sci.* **2018**, *5* (8), 1800222.
(53) Chang, C.; Tao, P.; Fu, B.; Xu, J.; Song, C.; Wu, J.; Shang, W.; Deng, T. Three-Dimensional Porous Solar-Driven Interfacial Evaporator for High-Efficiency Steam Generation under Low Solar Flux. *ACS Omega* **2019**, *4* (2), 3546−3555.
(54) Ni, G.; Zandavi, S. H.; Javid, S. M.; Boriskina, S. V.; Cooper, T. A.; Chen, G. A Salt-Rejecting Floating Solar Still for Low-cost Desalination. *Energy Environ. Sci.* **2018**, *11* (6), 1510−1519.

DOI: 10.1021/acsami.9b00380
ACS Appl. Mater. Interfaces 2019, 11, 15498−15506